Hydrodynamic instabilities of activity-balanced binary suspensions

Bryce Palmer, Wen Yan, and Tong Gao 1,3,*

¹Department of Mechanical Engineering, Michigan State University, East Lansing, Michigan 48864, USA
²Center for Computational Biology, Flatiron Institute, Simons Foundation, New York, New York 10010, USA
³Department of Computational Mathematics, Science and Engineering, Michigan State University,
East Lansing, Michigan 48864, USA



(Received 22 June 2021; accepted 7 June 2022; published 21 June 2022)

Microorganisms living in microfluidic environments often form multispecies swarms, where they can leverage collective motions to achieve enhanced transport and spreading. Nevertheless, there is a general lack of physical understandings of the origins of the multiscale unstable dynamics observed within these systems. In this study, we build a theoretical model to study the hydrodynamic instabilities arising in a dilute mixture of microswimmers that have different propulsion mechanisms and populations. Especially, we consider the scenario of an "activity-balanced" binary suspension that produces zero mean extra stress. We construct a continuum kinetic model that describes the transient dynamics as the system deviates from uniform isotropy. We perform linear stability analyses to show that such binary active suspensions may exhibit rich instability behavior that are far more complex than the single-species cases (e.g., pure pusher or puller suspensions) that have been well studied.

DOI: 10.1103/PhysRevFluids.7.063101

I. INTRODUCTION

Active suspensions of swimming microorganisms, such as bacteria or algae, can exhibit fascinating collective behavior that feature large-scale coherent structures, enhanced mixing, ordering transition, and anomalous diffusion [1,2]. In the limit of vanishing Reynolds numbers, self-driven or swimming microparticles effectively exert stresses upon the ambient liquid, which act as a coupling medium for the generation of large-scale collective dynamics. To uncover the multiscale origins of these unstable dynamics, researchers have constructed micromechanical models that can capture the distinctive swimming mechanisms for various microswimmers. Figure 1(a) sketches the so-called "pusher" and "puller" particles to characterize a class of microswimmers that respectively generate thrust at the rear (e.g., *E. coli*) and at the front (e.g., *Chlamydomonas*) of the body [3]. The swimming motions of such rodlike particles can produce dipolar extra stresses, the strength of which can be either negative (i.e., extensile) in the case of pushers or positive (i.e., contractile) in the case of pullers.

Thus far, our physical understanding of collective dynamics observed in active suspensions has been largely limited to the idealized situation of a single-particle species. In the dilute limit, it is well understood that pure pusher suspensions exert nonzero mean (or net) extensile stresses, which drive large-scale collective flows; on the other hand, net contractile stresses produced by pure puller suspensions suppress the development of active flows [1,4]. Nevertheless, in real-world ecosystems, multiple species of microorganisms may coexist with competition and coordination due to biological, chemical, and social mechanisms; these mixtures often utilize collective motions

^{*}gaotong@egr.msu.edu

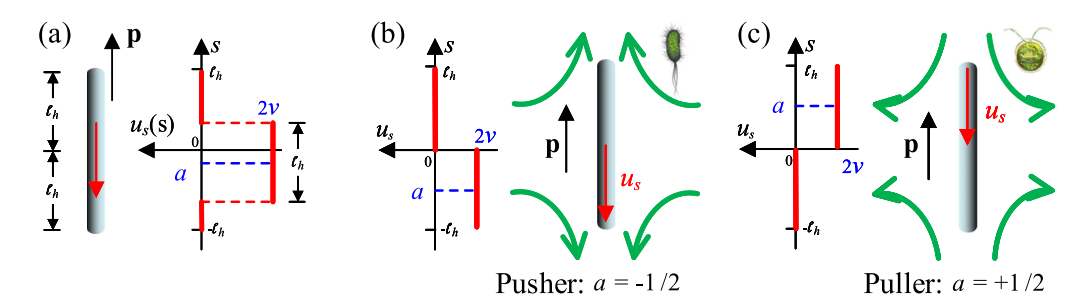


FIG. 1. (a) Schematic of active particles propelled by a step-like, backward (marked by the red arrow) slip velocity $u_s(s)$ projected along the centerline. Selecting different values of a can recover the classical (b) pusher (e.g., E. coli) and (c) puller (e.g., C. reinhardtii) model. In panels (b) and (c), the green arrows represent the resultant near-body flow directions.

to achieve efficient locomotion or spreading [5]. Several "dry" models that neglect hydrodynamic interactions have been used to study nonequilibrium phase transition and pattern formation of multispecies swarms [6–10]. Yet, far less is known about the role of fluid mechanics when different types of microswimmers interact collectively. Among the minimal studies of "wet" systems [11,12], we learn that the collective dynamics of pure pushers can be suppressed by adding pullers, or equivalently, adding contractile stresses, which effectively reduce or "neutralize" the extensile stresses produced by pushers. However, these studies only consider the simplest scenario of dilute binary suspensions where pushers and pullers have the same shape, population size, and swimming speed. In this scenario, the mean stress of the entire mixture exerted on the ambient fluid depends solely on the relative concentrations of the two species, as members of opposing species produce equal and opposite extra stresses.

In this study, we construct a minimal continuum model to investigate the origins of the unstable dynamics of a dilute mixture of pushers and pullers where the two types of microswimmers may have different swimming speeds, particle concentrations, and stress generation mechanisms. However, we subject the system to an "activity-balanced" condition such that the isolated stresslet produced by the two species exactly cancel one another. For dilute suspensions, this constraint effectively neutralizes the leading-order system stress leaving only higher-order stress fluctuations induced by the many-body interactions. Our key findings suggest that, even without mean extra stress generation, the interplay of the competing mechanisms—induced by differences in the stress generation, swimming speed, and relative particle number fractions—can drive rich hydrodynamic instabilities of both long- and finite-wavelength. We demonstrate that our model can recover the results of a reduced model of a symmetric pusher-puller mixture with a 1:1 ratio where all particles swim at the same speed with equal and opposite stress generation [12]. Moreover, our results suggest different instability mechanisms from those derived for pure pusher or pullers where a net extensile extra stress typically serves as the indicator of hydrodynamic instabilities or collective motions [4,13]. The paper is organized as follows: In Sec. II, we introduce the micromechanical models of active rodlike particles built upon the slender body theory. In Sec. III, we construct a mean-field kinetic model to describe the short-time, transient dynamics of dilute binary suspensions with an initially uniform isotropy configuration, and then set up the activity-balanced condition accordingly. In Sec. IV, we perform linear stability analyses to reveal the underlying instability mechanisms. Finally, we summarize and draw conclusions in Sec. V.

II. MICROMECHANICAL MODEL

Consider a dilute suspension of slender active rods. Each rod has an equal length ℓ and diameter b with aspect ratio $r = \ell/b \gg 1$. To model particle activity, we assume the self-swimming motion

is actuated by a slip velocity distribution on the particle's surfaces. For microrods with high aspect ratios, we neglect the particle thickness and project the surface slip velocity onto the rod's center-line along the local arclength $s \in [-\ell_h, \ell_h]$ (ℓ_h is the rod's half length). As sketched in Fig. 1, we choose the slip velocity distribution $u_s(s)$ to be a simple step function with a fixed width ℓ_h and magnitude 2v. Specifically,

$$u_s(s) = \begin{cases} 0, & -\ell_h \leqslant s < \ell_h(a - 1/2) \\ 2\nu, & \ell_h(a - 1/2) \leqslant s \leqslant \ell_h(a + 1/2) \\ 0, & \ell_h(a + 1/2) < s \leqslant \ell_h. \end{cases}$$
(1)

Note, we choose $u_s < 0$ and correspondingly v < 0 such that the particle will swim in the forward direction. The centroid location a of the "active segment" characterizes the symmetry of surface actuation, which directly determines the magnitude and sign of the produced stress without varying the isolated swimming speed. It is straightforward to show that selecting a negative value of a, i.e., $a \in [-1/2, 0]$, corresponds to a pusher-type particle that is predominately actuated from the rear and generates a local extensile flow field. Likewise, selecting a positive value of a, i.e., $a \in [0, +1/2]$, corresponds to a puller-like particle, a mostly head-actuated particle with a local contractile flow profile. We emphasize that this definition for pusher and puller is broader than the classical definition [3] [see the schematics in Figs. 1(b) and 1(c)], which typically refers to particles that are entirely driven by their front-half (i.e., a = +1/2) or rear-half (i.e., a = -1/2). By allowing for |a| < 1/2, we consider a broader class of pushers and pullers with reduced stress asymmetry.

Following the classical slender body theory [14,15], we denote the unknown force distribution along the particle centerline as $f^e(s)$ and the induced disturbance velocity due to the many-body hydrodynamic interactions as $u_{\infty}(s)$. For rods with the center-of-mass (C.O.M.) position x and orientation along the unit vector p(|p| = 1), the relation between particle motion and force distribution can then be formulated as

$$\dot{\mathbf{x}} + s\dot{\mathbf{p}} + u_s(s)\mathbf{p} - \mathbf{u}_{\infty}(s) = c(\mathbf{I} + \mathbf{p}\mathbf{p}) \cdot f^e(s), \tag{2}$$

where the hydrodynamic force distribution $f^e(s)$ satisfies the force- and torque-free conditions $\int_{-\ell_h}^{\ell_h} f^e(s) ds = \mathbf{0}$ and $\int_{-\ell_h}^{\ell_h} s p \times f^e(s) ds = \mathbf{0}$ and $c = \ln(2r)/4\pi\mu$ is an effective drag coefficient. By taking the first and second moments of the orthonormal projection of (2) onto the parallel and perpendicular directions to p, we can analytically solve $f^e(s)$ for an isolated particle [i.e., $u_{\infty}(s) = \mathbf{0}$]. In turn, we find that an isolated particle will swim with a certain speed v and produce dipolar extra stress $\sigma_0 pp$ [16]. The coefficient σ_0 —the so-called "stresslet"—has a unit of force times length and can be defined as

$$\sigma_0 = -\frac{1}{2c} \int_{-\ell_*}^{\ell_h} s u_s(s) ds = \frac{-va\ell_h^2}{c}.$$
 (3)

This equation reveals that the stress generated by a motile, slender particle with slip distribution (1) is jointly determined by the particle's motility and the asymmetry of the imposed surface actuation (i.e., in terms of a). The stresslet strength generated by each particle may, therefore, be modulated independent of the particle's isolated swimming speed by modifying a; however, varying particle motility will directly lead to a change in stress. More general active particle models can be constructed such that the particle stress and the swimming speed are completely decoupled [17].

III. MEAN-FIELD KINETIC MODEL

Now, consider N rigid active rods—as described in Sec. II—suspended in a cubic periodic domain with width L and volume $V = L^3$. Among them, we assume there are N^+ pushers and $N^- = N - N^+$ pullers, with corresponding number fraction $\chi = N^+/N$ for pushers and $1 - \chi = N^-/N$ for pullers. Hereafter, we will use superscripts $^+$ and $^-$ to denote quantities for the pushers and pullers, respectively, such as the swimming speed v^{\pm} and actuation asymmetry a^{\pm} . Also, to

facilitate analysis, we introduce the universal characteristic velocity scale $u_c = (v^+ + v^-)/2$ for the entire mixture from which we obtain the speed ratio $\gamma^{\pm} = v^{\pm}/u_c$ for each species.

Next, we construct a minimal continuum model by extending the classical mean-field kinetic model for a single-species [4] to the case of binary suspensions, aiming to capture the key flow physics as the system dynamics deviate from a uniform isotropy. To begin with, we describe the continuum configuration of the mixed species using the probability distribution functions (PDFs) $\Psi^{\pm}(x, p, t)$ in terms of the rods' C.O.M. position x and orientation p, with the superscript " \pm " consistent with micromechanical model above. As an expression of the conservation of particle number, one can derive the Smoluchowski equations

$$\frac{\partial \Psi^{\pm}}{\partial t} + \nabla \cdot (\dot{\mathbf{x}}^{\pm} \Psi^{\pm}) + \nabla_{\mathbf{p}} \cdot (\dot{\mathbf{p}}^{\pm} \Psi^{\pm}) = 0, \tag{4}$$

where ∇ is the regular spatial gradient operator and $\nabla_p = (\mathbf{I} - pp) \cdot \partial/\partial p$ is the orientational gradient operator on the unit sphere. For both species, their PDFs satisfy the global constraints

$$\frac{1}{V} \int_{V} \int_{S} \Psi^{+}(\boldsymbol{x}, \boldsymbol{p}, t) dS_{p} dV = \chi, \quad \frac{1}{V} \int_{V} \int_{S} \Psi^{-}(\boldsymbol{x}, \boldsymbol{p}, t) dS_{p} dV = 1 - \chi, \tag{5}$$

with χ being the number fraction. We also define the zeroth (i.e., concentration) and the second moment of Ψ as

$$c^{\pm}(\boldsymbol{x},t) = \int_{S} \Psi^{\pm}(\boldsymbol{x},\boldsymbol{p},t) dS_{p}, \quad \boldsymbol{D}^{\pm}(\boldsymbol{x},t) = \int_{S} \Psi^{\pm}(\boldsymbol{x},\boldsymbol{p},t) \boldsymbol{p} \boldsymbol{p} dS_{p}. \tag{6}$$

Then, we can derive the conformational fluxes \dot{x}^{\pm} and \dot{p}^{\pm} using local slender-body theory as

$$\dot{\mathbf{x}}^{\pm} = \gamma^{\pm} \mathbf{p} + \mathbf{u} - d_T^{\pm} \nabla (\ln \Psi^{\pm}), \tag{7}$$

$$\dot{\mathbf{p}}^{\pm} = (\mathbf{I} - \mathbf{p}\mathbf{p}) \cdot \nabla \mathbf{u} \cdot \mathbf{p} - d_{R}^{\pm} \nabla_{\mathbf{p}} (\ln \Psi^{\pm}). \tag{8}$$

Equations (7) and (8) state that an individual particle can move at a speed of $\gamma^{\pm}p$ relative to the background mean-field fluid velocity u, which plays the same role as u_{∞} in Eq. (2), and simultaneously rotate under the fluid shear by following Jeffrey's orbit [18]. These equations are nondimensionalized according to the universal characteristic velocity scale u_c and length scale $\ell_c = (n\ell^2)^{-1}$ with n = N/V the total particle number density. In addition to the deterministic motions, diffusion effects in binary suspensions are incorporated via the dimensionless isotropic translational (d_T^{\pm}) and rotational (d_R^{\pm}) diffusion coefficient. It is worthwhile mentioning that this model also somewhat resembles the "cyclic swimmers" model proposed in Ref. [13] in mimicking a class of particles undergoing transitions between pusher and puller states.

The above equations are closed by solving the incompressible fluid velocity u that is produced by the extra-stress tensor Σ , which is, in turn, produced by the particles' presence via a forced Stokes equation

$$\nabla p - \nabla^2 \mathbf{u} = \nabla \cdot \mathbf{\Sigma},\tag{9}$$

$$\nabla \cdot \boldsymbol{u} = 0, \tag{10}$$

where p is the fluid pressure. The extra stress includes both species' contributions and sums the single stresslet $\sigma_0 pp$ for all particles. Then, following the Kirkwood theory [19], we derive the two configurational-averaged stresses as

$$\boldsymbol{\Sigma}^{\pm}(\boldsymbol{x},t) = \alpha^{\pm} \int_{S} \Psi^{\pm} \boldsymbol{p} \boldsymbol{p} dS_{p} = \alpha^{\pm} \boldsymbol{D}^{\pm}(\boldsymbol{x},t), \tag{11}$$

with the strength coefficients

$$\alpha^{\pm} = \frac{\pi \gamma^{\pm} a^{\pm}}{\log (2r)} \propto \gamma^{\pm} a^{\pm} \begin{cases} < 0, & \text{Pusher (+)} \\ > 0, & \text{Puller (-),} \end{cases}$$
 (12)

leading to the total stress

$$\Sigma = \chi \Sigma^{+} + (1 - \chi)\Sigma^{-} = \alpha^{+} \chi \mathbf{D}^{+}(\mathbf{x}, t) + \alpha^{-}(1 - \chi)\mathbf{D}^{-}(\mathbf{x}, t). \tag{13}$$

Note that defining local total stress in (13) requires applying appropriate ensemble averaging in a certain small representative elementary volume, whose size needs to be selected based on the characteristic features of the bulk material properties. As well, during the initial transient period, when the system dynamics just start to deviate from the initial uniform isotropic state, Σ in (13) can be defined globally. We also assume that the binary suspension is dilute and therefore consider contributions due to short-range steric interactions (e.g., collisions) to be negligible.

To derive the activity-balance condition from the above governing equations, we first perturb the initial equilibrium solution of an isotropic state by incorporating the disturbance solutions that fluctuate around their global means, i.e., $\Psi^{\pm} = 1/4\pi + \epsilon \Psi'_{\pm}$ and $\mathbf{u} = \epsilon \mathbf{u}'$ ($|\epsilon| \ll 1$). Here, we use superscript "," to denote all high-order disturbance solutions hereinafter. We can calculate the following near-isotropy expansions

$$\frac{c^{+}(\mathbf{x},t)}{\chi} = 1 + \epsilon c'_{+}(\mathbf{x},t), \quad \frac{c^{-}(\mathbf{x},t)}{1-\chi} = 1 + \epsilon c'_{-}(\mathbf{x},t), \tag{14}$$

$$\boldsymbol{D}^{\pm}(\boldsymbol{x},t) = \frac{\mathbf{I}}{3} + \epsilon \boldsymbol{D}_{\pm}'(\boldsymbol{x},t). \tag{15}$$

Then the stress defined in Eq. (13) can be written as

$$\Sigma(x,t) = [\alpha^{+} \chi + \alpha^{-} (1-\chi)] \mathbf{I} + \epsilon \Sigma'.$$
 (16)

The prefactor $\alpha^+ \chi + \alpha^- (1 - \chi)$ essentially characterizes the mean activity for a homogeneous system. Thus, eliminating the extra stress at the leading order yields the activity-balanced condition

$$\chi = \frac{-\alpha^{-}}{\alpha^{+} - \alpha^{-}} = \frac{-\gamma^{-}a^{-}}{\gamma^{+}a^{+} - \gamma^{-}a^{-}}, \quad 1 - \chi = \frac{\alpha^{+}}{\alpha^{+} - \alpha^{-}} = \frac{\gamma^{+}a^{+}}{\gamma^{+}a^{+} - \gamma^{-}a^{-}}.$$
 (17)

IV. LINEAR STABILITY ANALYSIS

It is straightforward to perform the linear stability analysis for the governing equations (4)–(13) when subjected to the activity-balanced condition (17). Using the equilibrium condition in (17), we can perturb the isotropic base-state PDF solutions with disturbance functions Ψ'_{+} as

$$\Psi^{\pm} = \mp \frac{\alpha^{\mp}}{4\pi(\alpha^{+} - \alpha^{-})} (1 + \epsilon \Psi'_{\pm}), \tag{18}$$

which, together with the distance fluid velocity u', lead to the linearized Smoluchowski equations

$$\frac{\partial \Psi'_{\pm}}{\partial t} = -\gamma^{\pm} \boldsymbol{p} \cdot \nabla \Psi'_{\pm} + d_T^{\pm} \nabla^2 \Psi'_{\pm} + 3 \boldsymbol{p} \boldsymbol{p} : \boldsymbol{E}', \tag{19}$$

with $E' = (\nabla u' + \nabla u'^T)/2$ the strain-rate tensor. Then, we follow Ref. [4] to apply a plane-wave decomposition to the disturbance functions such that

$$\Psi'_{\pm}(\mathbf{x}, \mathbf{p}, t) = \widetilde{\Psi}^{\pm}(\mathbf{p}, \mathbf{k}) \exp(i\mathbf{k} \cdot \mathbf{x} + \sigma t), \tag{20}$$

$$\mathbf{u}'(\mathbf{x},t) = \widetilde{\mathbf{u}}(\mathbf{k}) \exp(i\mathbf{k} \cdot \mathbf{x} + \sigma t), \tag{21}$$

$$c'(\mathbf{x},t) = \widetilde{c}(\mathbf{k}) \exp(i\mathbf{k} \cdot \mathbf{x} + \sigma t), \tag{22}$$

where k is the wave vector and σ is the growth rate. Both scalar and vector Fourier coefficients that are denoted with " \sim " can then be solved by converting the above linear equations to Fourier space, yielding

$$\tilde{\Psi}^{\pm} = -\frac{(\boldsymbol{p} \cdot \hat{\boldsymbol{k}})}{\sigma + k^{2} d_{T}^{\pm} + i \gamma^{\pm} (\hat{\boldsymbol{k}} \cdot \boldsymbol{p})} \boldsymbol{p} \cdot (\boldsymbol{I} - \hat{\boldsymbol{k}} \hat{\boldsymbol{k}}) \cdot \tilde{\boldsymbol{\Sigma}} \cdot \hat{\boldsymbol{k}}$$

$$= \frac{3\alpha^{+} \alpha^{-}}{4\pi (\alpha^{+} - \alpha^{-})} \frac{(\boldsymbol{p} \cdot \hat{\boldsymbol{k}}) \boldsymbol{p} \cdot [\boldsymbol{F}(\tilde{\boldsymbol{\Psi}}_{+}) - \boldsymbol{F}(\tilde{\boldsymbol{\Psi}}_{-})]}{\sigma + k^{2} d_{T}^{\pm} + i \gamma^{\pm} (\hat{\boldsymbol{k}} \cdot \boldsymbol{p})}, \tag{23}$$

where $\hat{k} = k/|k|$ is a unit wave vector. In deriving Eq. (23), we follow [4] to define the operator $F(\tilde{\Psi}^{\pm}) = (I - \hat{k}\hat{k}) \cdot \int_{S} p(p \cdot \hat{k}) \widetilde{\Psi}^{\pm} dS_{p}$ and solve the fluid disturbance velocity in Fourier space as

$$\tilde{\boldsymbol{u}} = \frac{i}{k} (\boldsymbol{I} - \hat{\boldsymbol{k}}\hat{\boldsymbol{k}}) \cdot \tilde{\boldsymbol{\Sigma}} \cdot \hat{\boldsymbol{k}}, \tag{24}$$

through which the two species interact with each other hydrodynamically. Applying the operator of $F(\tilde{\Psi}^{\pm})$ on both sides of Eq. (23) yields two coupled equations, from which we can solve the eigenvalue problem to obtain the dispersion relation

$$(1 - \chi) \left[2\zeta_{-}^{3} - \frac{4\zeta_{-}}{3} + (\zeta_{-}^{4} - \zeta_{-}^{2}) \log \left(\frac{\zeta_{-} - 1}{\zeta_{-} + 1} \right) \right] + \chi \left[2\zeta_{+}^{3} - \frac{4\zeta_{+}}{3} + (\zeta_{+}^{4} - \zeta_{+}^{2}) \log \left(\frac{\zeta_{+} - 1}{\zeta_{+} + 1} \right) \right] + \frac{4ik}{3} = 0,$$
(25)

where $\zeta_{\pm} = -i(\sigma + k^2 d_T^{\pm})/(k\gamma^{\pm})$. Furthermore, we note that the mathematical formulation of Eq. (23) suggest all the eigenmodes in Fourier space to take the following form:

$$\tilde{\Psi}^{\pm} \propto \frac{3\alpha^{+}\alpha^{-}}{4\pi(\alpha^{+} - \alpha^{-})} \left(\frac{(\boldsymbol{p} \cdot \hat{\boldsymbol{k}})(\boldsymbol{p} \cdot \hat{\boldsymbol{k}}_{\perp})}{\sigma + k^{2}d_{T}^{\pm} + i\gamma^{\pm}(\hat{\boldsymbol{k}} \cdot \boldsymbol{p})} \right), \tag{26}$$

with \hat{k}_{\perp} being a unit vector perpendicular to \hat{k} . Without loss of generality, we can choose the spherical coordinates with polar axis as $\hat{z} = \hat{k}$, and the orientation vector can be written as $p = [\sin\theta\cos\phi, \sin\theta\sin\phi, \cos\theta]$ [4]. It is straightforward to show that the concentration and polarity disturbances (i.e., the 0th and 1st moments of Ψ') become zero. Only the disturbance solution of active stress Σ' which is equivalent to the 2nd moment of Ψ' could have nonzero off-diagonal terms, with the corresponding eigenvector mode being written as $\hat{k}\hat{k}_{\perp} + \hat{k}_{\perp}\hat{k}$. In other words, any instabilities captured by the following analysis can be reflected in the active stress or nematic order at the macro scale.

Instead of simultaneously varying all the parameters in (25), we first focus on the scenario when the pushers and pullers have the same actuation asymmetry, i.e., $-a^+ = a^-$, such that the instability is purely driven by particle motility γ^\pm and relative number fraction χ according to the stress balanced condition, Eq. (17). As shown in Figs. 2(a) and 2(b), where the classical pusher-puller model is recovered by selecting $-a^+ = a^- = 1/2$, we can numerically solve three solution branches for the real part of the growth rate Re(σ) from Eq. (25) at different values of χ when neglecting diffusion ($d_T^\pm = d_R^\pm = 0$). At $\chi > 0.5$ when the slow-moving pushers outnumber the fast-moving pullers, the two solid branches on the top are unstable, while the third dashed branch with negative values is stable. Although there is no diffusion added, the system has intrinsic mechanisms for damping fluctuations at large k, yielding a cutoff wave number k_c beyond which all fluctuations become damped. Starting from χ close to 1, we observe the Re(σ) decreasing as χ decreases, with a smaller and smaller k_c , until Re(σ) drops to zero at $\chi = 0.5$, which is consistent with the prediction of stable symmetric binary mixture with effectively noninteracting particles by Bárdfalvy *et al.* [12]. As χ further decreases, we find the corresponding solutions marked by blue lines are exactly the mirror images with respect to the k axis of those marked by red computed at $1 - \chi$, meaning that

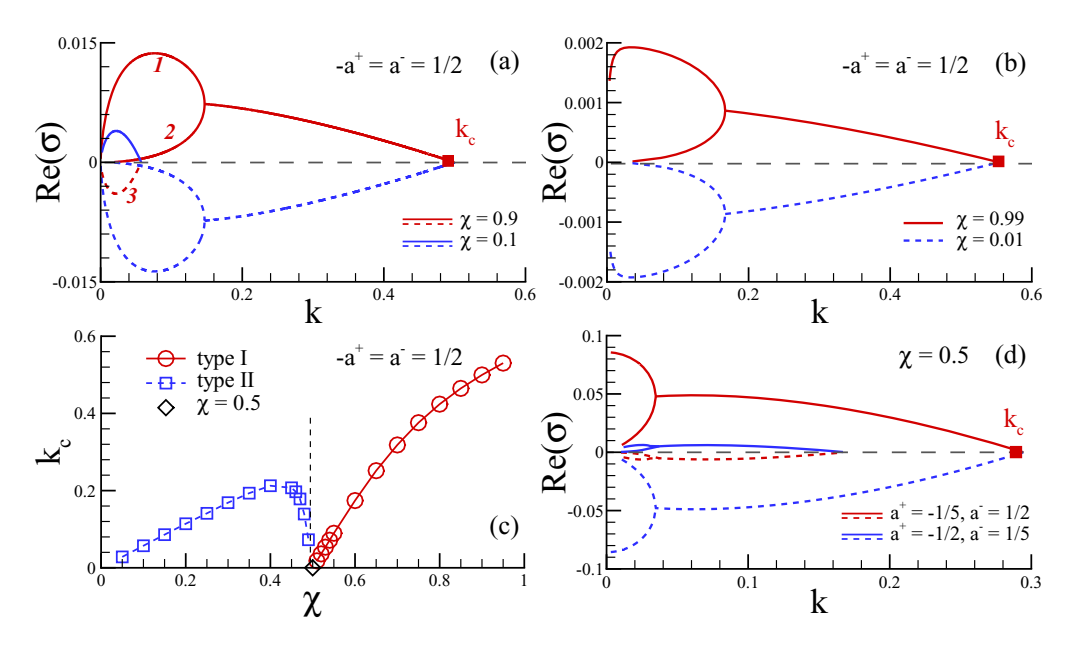


FIG. 2. Linear stability analysis for activity-balanced binary mixtures when (a)–(c) fixing $-a^+ = a^-$ and varying γ^{\pm} (hence χ), or (d) fixing χ but allowing $-a^+ \neq a^-$. (a), (b), (d) Growth rate Re(σ) as a function of wave number k. The solid and dashed lines respectively represent the positive and negative growth rates. (c) The critical wave number k_c as a function of χ for the "puller-faster" (type I) and "pusher-faster" (type II) cases when fixing $-a^+ = a^- = 1/2$.

all stable (unstable) solutions are now flipped to become unstable (stable). As a result, instabilities, while weak, may occur even when there are more pullers than pushers.

To make comparison with the classical kinetic model for pure pushers and pullers, we analyze the limiting behavior of our model as χ approaches 0 or 1 with $-a^+ = a^- = 1/2$. Note that at the extrema of $\chi = 0$ or 1, the activity-balanced condition from Eq. (17) requires that the particles have zero isolated swimming speed. This is unsurprising, as the only activity-balanced case within a single species suspension is that of a passive system. As demonstrated in Fig. 2(b), the magnitude of this finite wavelength instability decreases to zero in the limit as $\chi \to 0$ or 1, indicating that the system is stable. At this limit, the wave number of the maximum growth-rate tends to zero and k_c tends to 0.55, which suggests that we recover the long-wavelength instability and critical wave number discussed in Refs. [1,4] for a single species.

The sign-flipping of the stable-unstable solutions shown in Figs. 2(a) and 2(b) effectively leads to nonmonotonic variation of k_c when plotted as a function of χ in Fig. 2(c). We observe that k_c first increases with χ and then quickly drops to zero at $\chi=0.5$ when symmetric binary suspensions are stable; when χ further increases, k_c grows from zero again. Therefore, $\chi=0.5$ with $\gamma^+=\gamma^-$ defines a critical point of a first-order transition between the two types of hydrodynamic instabilities. First, instability may arise because of a larger number of pushers, albeit moving slowly, which we referred to as the "puller-faster" (type I) cases. Although the shape of the unstable branches (solid red lines) resemble those obtained for the single-species suspensions of pure pushers [4], the maximum growth rates we obtained are one order of magnitude lower, which hence suggests much weaker instabilities. Also, these instabilities are of finite-wavelength with the maximum growth rate occurring at k>0, compared with the long-wave instabilities for pure pushers [4,20]. Second, the kinetic model suggests that at small values of χ when slow pullers outnumber fast pushers, instabilities may still occur, hence referred to as the "pusher-faster" (type II) cases that are marked by the blue color. However, it deserves mention that, in this scenario, instabilities are generally weaker than type-I cases, typically with much smaller maximum growth rates and smaller k_c . In addition,

it is worthwhile to mention that when the two species swim at the same speed, i.e., $\gamma^+ = \gamma^- = \gamma$ and neglecting diffusion, apparently $\zeta_+ = \zeta_- = \zeta$. Hence Eq. (25) further simplifies to

$$\left[2\zeta^{3} - \frac{4\zeta}{3} + (\zeta^{4} - \zeta^{2})\log\left(\frac{\zeta - 1}{\zeta + 1}\right)\right] + \frac{4ik}{3} = 0.$$
 (27)

We find these cases are always stable, independent of fraction number and actuation type. We emphasize that the instabilities discussed above are not caused by particle motility alone; instead, particle motility is directly coupled to the generated stress, according to Eq. (3). By introducing actuation asymmetry in the particle geometry, one may study the impacts of different swimming speeds without coupling velocity and stress together. For example, Škultéty *et al.* [17] studied how various correlation functions are impacted by particle self-propulsion when particle stress is held constant.

We now focus on the scenario when the pushers and pullers have fixed concentration but $-a^+ \neq a^-$, such that the stresslet strength generated by each species is no longer equal and opposite. Figure 2(d) shows the results when $\chi=0.5$. In this case, the solution curves once again show mirror-image symmetry; although, the symmetry is now achieved when $-a^+_{(1)} = a^-_{(2)}$ and $a^-_{(1)} = -a^+_{(2)}$. In fact, this sign flipping exactly corresponds to the case when $\gamma^+ = \gamma^-$ given in Eq. (27), which is guaranteed to be stable regardless of χ or a^+, a^- . Interestingly, the positive growth rate with Fig. 2(d) shows that the neutrally stable case at $\chi=0.5$ in Fig. 2(c) now becomes unstable due to each species swimming at different velocities to counteract the difference in stress magnitudes. As well, the solid red line, corresponding to the "pusher-faster" case, exhibits a strong long-wavelength instability with the maximum growth rate occurring at k=0; while the solid blue line, corresponding to the "puller-faster" case, retains the feature of finite-wavelength instability. These maximum growth rates are far stronger than those seen when $a^+=a^-$ in Figs. 2(a) and 2(b). It deserves to be mentioned the simultaneously varying concentration, isolated swimming speed, and surface actuation type yields complex, nonlinear behavior that are difficult to be summarized to show clear trends like those seen in Figs. 2(a)–2(c).

V. CONCLUSION AND DISCUSSION

To summarize, we have built a theoretical framework to study the underlying hydrodynamic instabilities in dilute, activity-balanced pusher-puller binary suspensions that produce near zero mean extra stress. By building a mean-field kinetic model, we have successfully demonstrated that in such binary systems, mixing pushers and pullers may lead to much richer behavior than a simple neutralization processes as a result of the cancellation of stresslets from both species. Even without producing mean extra stresses, hydrodynamic instabilities can still grow from a uniform isotropic state, suggesting that nonzero mean extensile stress is not necessarily a sufficient indicator of collective motions. The linear stability analyses near uniform isotropy have captured various types of hydrodynamic instabilities which reveal the possible origins of the unstable dynamics. It will be also intriguing to further verify our theoretical predictions by examining with the growth of the orientation moments measured in discrete particle simulations or experiments to identify the instability type.

Besides, we expect this work to initiate new studies of measuring, characterizing, and predicting the complex dynamics in multispecies-multicomponent active systems. Especially considering the high computation costs of large-scale discrete particle simulations, of particular interest will be developing more accurate continuum models that can fully resolve the late-time nonlinear dynamics arising from nonequilibrium, inhomogeneous mixtures. As discussed in Sec. III, one key step in mean-field models like ours is constructing a local total extra stress [i.e., Σ in Eq. (13)] to drive active flows and account for inhomogeneity. Besides formulating the concentration-dependent dipolar stresses (note that D scales with the local concentration c), we need to evaluate Σ based on a certain local fractional number, e.g., $\chi^{\pm}(x) = c^{\pm}/(c^{+} + c^{-})$, instead of simply treating χ as a

constant global mean. Alternatively, one may choose the kinetic model developed by Škultéty *et al.* [17] that avoids to use mean-field approaches for modeling the many-body interactions via directly constructing extra stresses. In their method, microparticles are treated as simple point dipoles. Then the induced hydrodynamic effects are evaluated by summing individual dipolar stresses via regularized Stokeslets. More computation studies of binary mixtures using continuum models, together with detailed comparisons with discrete particle simulations, will be presented in the future.

ACKNOWLEDGMENT

This work is supported by NSF Grant No. CAREER-1943759.

- [1] S. Ramaswamy, The mechanics and statistics of active matter, Annu. Rev. Condens. Matter Phys. 1, 323 (2010).
- [2] M. Shelley, The dynamics of microtubule/motor-protein assemblies in biology and physics, Annu. Rev. Fluid Mech. 48, 487 (2016).
- [3] T. Ishikawa, M. Simmonds, and T. Pedley, Hydrodynamic interaction of two swimming model microorganisms, J. Fluid Mech. 568, 119 (2006).
- [4] D. Saintillan and M. Shelley, Instabilities, pattern formation, and mixing in active suspensions, Phys. Fluids 20, 123304 (2008).
- [5] E. Ben-Jacob, A. Finkelshtein, G. Ariel, and C. Ingham, Multispecies swarms of social microorganisms as moving ecosystems, Trends Microbiol. 24, 257 (2016).
- [6] R. Wittmann, J. M. Brader, A. Sharma, and U. M. B. Marconi, Effective equilibrium states in mixtures of active particles driven by colored noise, Phys. Rev. E 97, 012601 (2018).
- [7] R. Maloney, G. Liao, S. Klapp, and C. Hall, Clustering and phase separation in mixtures of dipolar and active particles, Soft Matter 16, 3779 (2020).
- [8] J. Stenhammar, R. Wittkowski, D. Marenduzzo, and M. E. Cates, Activity-Induced Phase Separation and Self-Assembly in Mixtures of Active and Passive Particles, Phys. Rev. Lett. 114, 018301 (2015).
- [9] T. Kolb and D. Klotsa, Active binary mixtures of fast and slow hard spheres, Soft Matter 16, 1967 (2020).
- [10] S. Takatori and J. Brady, A theory for the phase behavior of mixtures of active particles, Soft Matter 11, 7920 (2015).
- [11] G. Pessot, H. Löwen, and A. M. Menzel, Binary pusher-puller mixtures of active microswimmers and their collective behaviour, Mol. Phys. 116, 3401 (2018).
- [12] D. Bárdfalvy, S. Anjum, C. Nardini, A. Morozov, and J. Stenhammar, Symmetric Mixtures of Pusher and Puller Microswimmers Behave as Noninteracting Suspensions, Phys. Rev. Lett. 125, 018003 (2020).
- [13] T. Brotto, D. Bartolo, and D. Saintillan, Spontaneous flows in suspensions of active cyclic swimmers, J. Nonlinear Sci. 25, 1125 (2015).
- [14] G. Batchelor, Slender-body theory for particles of arbitrary cross-section in Stokes flow, J. Fluid Mech. 44, 419 (1970).
- [15] D. Saintillan and M. Shelley, Emergence of coherent structures and large-scale flows in motile suspensions, J. R. Soc. Interface 9, 571 (2012).
- [16] C. Hohenegger and M. J. Shelley, Dynamics of complex biofluids, in *New Trends in the Physics and Mechanics of Biological Systems*, Lecture Notes of the Les Houches Summer School, Vol. 92 (Oxford University Press, 2011).
- [17] V. Škultéty, C. Nardini, J. Stenhammar, D. Marenduzzo, and A. Morozov, Swimming Suppresses Correlations in Dilute Suspensions of Pusher Microorganisms, Phys. Rev. X 10, 031059 (2020).
- [18] G. Jeffery, The motion of ellipsoidal particles immersed in a viscous fluid, Proc. R. Soc. London, Ser. A 102, 161 (1922).
- [19] M. Doi and S. Edwards, The Theory of Polymer Dynamics (Oxford University Press, 1988).
- [20] R. Simha and S. Ramaswamy, Statistical hydrodynamics of ordered suspensions of self-propelled particles: Waves, giant number fluctuations and instabilities, Phys. A (Amsterdam, Neth.) 306, 262 (2002).